Thermomechanics failure of RC composites: computational approach with enhanced beam model

Minh Ngo[1,3a], Adnan Ibrahimbegovic[*1] and Delphine Brancherie[2b]

[1]*École Normale Supérieure, Laboratory of Mechanics and Technology-Cachan, France*
[2]*Université de Technologie de Compiègne, Laboratory Roberval, France*
[3]*University of Communications and Transport, Department of Civil Engineering, Vietnam*

Abstract.   In this paper we present a new model for computing the nonlinear response of reinforced concrete frame systems subjected to extreme thermomechanical loads. The first main feature of the model is its ability to account for both bending and shear failure of the reinforced concrete composites within frame-like model. The second prominent feature concerns the model capability to represent the total degradation of the material properties due to high temperature and the thermal deformations. Several numerical simulations are given to confirm these capabilities and illustrate a very satisfying model performance.

Keywords: thermomechanics failure; timoshenko beam; enhanced finite element

1. Introduction

The mechanical response of reinforced concrete frame structure at elevated temperature were studied by many researchers and a number of interesting methods were introduced in Capua and Mari (2007), Kodur and Dwaikat (2008), Dwaikat and Kodur (2008), Xavier (2009), ACI-216 (1997). Most of these previous studies considered only the bending response and ignored the shear behavior, which is also a typical damage model of the reinforced concrete structure. Moreover, practically none of the works available in the literatures considers the effect of shear force and axial force on the bending resistance of reinforced concrete element, although the stress-strain relation typical of the cross-section where shear force and axial force exist are much different to the stress/strain condition in the pure bending cross-section. Another deficiency of previously proposed methods is that they take into account only the degradation of the mechanical resistance due to material strength reduction at high temperature, while the 'thermal' response of the frame is usually neglected. However, at high temperature, thermal behavior might contribute a significant amount to the total behavior of the section. The last important model feature to be improved with respect to the previous works is to cast the stress-resultant model that can represent such a

∗Corresponding author, Professor, E-mail: ai@lmt.ens-cachan.fr
[a] Ph. D., E-mail: minhngovan83@gmail.com
[b] Ph. D., E-mail: delphine.brancherie@utc.fr

thermomechanical behavior of a reinforced concrete elements (either beam or column), which can provide an efficient computational basis in identifying the overall response of the frame structure.

The outline and main contributions of this paper are as follows. In the first part of this article, we studied the degradation of mechanical resistance of the reinforced concrete cross-section under bending moment, shear force and axial loading due to temperature increase. These degradations was studied based on the 'layer' method in the framework of Modified Compression Theory proposed by Vecchio and Collins (1988), Vecchio and Emara (1992), Bentz *et al*. (2006) but was extended to include the temperature dependence of material properties and the stress-strain condition due to thermal loading. In such a method, the cross-section is divided into layers, which are small enough to assume uniform stress and strain condition and constant temperature through the layer thickness. In that way, the reduction of material properties due to temperature at each layer is considered and accumulated into the degradation of overall resistance of the cross-section. The thermal strain due to temperature gradient at each layer is also taken into account to estimate the total deformation of the cross-section and to compute the total stress in each layer. The latter contributes in total response of the section, especially for high temperature typical of fire loading.

In the second part of the paper, we introduce the finite element method to provide an efficient computational framework using the stress-resultant constitutive model of reinforced concrete beam element. The latter is then used for limit load computations of the reinforced concrete frame structures subjected to combined mechanical loading and fire.

2. Stress-resultant model of a reinforced concrete beam element subjected to mechanical and thermal loads

In this section, we present how the modified compression theory is adapted to derive the stress-resultant model desciribing the behavior of a beam cross-section submitted to mechanical and thermal loading. In particular, we present the evolution of the mechanical parameters entering the stress-resultant model in terms of the temperature.

2.1 Stress and strain condition at a position in reinforced concrete beam element under mechanical and temperature loading

Fig. 1 Mechanical loading and fire acting on reinforced concrete element

Consider a reinforce concrete beam element subjected to mechanical loading and thermal loading (see Fig. 1).

Table 1 List of symbols for thermomechanical model

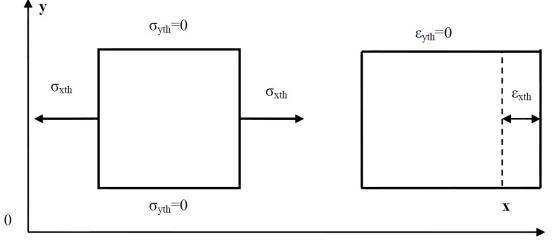| Symbol	Meaning
θ	Angle of principal direction (for both deformation and stress condition)
σ_x	Normal stress in x direction (longitudinal direction)
σ_y	Normal stress in y direction (tranverse direction)
τ	Shear stress
σ_1	1st (maximum) principal stress
σ_2	2nd (minimum) principal stress
ε_{xm}	Mechanical normal strain in x direction (longitudinal direction)
ε_{ym}	Mechanical normal strain in y direction (tranverse direction)
γ	Shear strain
ε_1	1st (maximum) principal strain
ε_2	2nd (minimum) principal strain
σ_{xt}	Thermal stress in x direction (longitudinal direction)
ε_{xth}	Thermal strain in x direction (longitudinal direction)

Fig. 2 Thermal stress and thermal strain condition

In this element, beside the mechanical deformation, a thermal strain is also acting. The total strain is then the sum of mechanical strain and thermal strain

$$\varepsilon = \varepsilon_m + \varepsilon_{th} \qquad (1)$$

Fig. 2 represents the thermal stress and strain condition at a given point in the element.

The thermal strain of concrete depends on the temperature and the kind of aggregates EN-1992-1-2 (2004), such that we have for calcareous aggregates

$$\varepsilon_{cth}(T) = \begin{cases} -1.2 \times 10^{-4} + 6 \times 10^{-6} T + 1.4 \times 10^{-11} T^3 & for \quad 20^0 C \le T \le 805^0 C \\ 12 \times 10^{-3} & for \quad T > 805^0 C \end{cases} \qquad (2)$$

for siliceous aggregates

$$\varepsilon_{cth}(T) = \begin{cases} -1.8 \times 10^{-4} + 9 \times 10^{-6} T + 2.3 \times 10^{-11} T^3 & for \quad 20^0 C \le T \le 700^0 C \\ 14 \times 10^{-3} & for \quad 700^0 C \le T \le 1200^0 C \end{cases} \qquad (3)$$

The thermal strain of steel also depends on the temperature (EN-1992-1-2 2004)

$$\varepsilon_{sth} = \begin{cases} -2.416 \times 10^{-4} + 1.2 \times 10^{-5} T + 0.4 \times 10^{-8} T^2 & for \quad 20^0 C \le T \le 750^0 C \\ 11 \times 10^{-3} & for \quad 750^0 C < T \le 860^0 C \\ -6.2 \times 10^{-3} + 2 \times 10^{-5} T & for \quad 860^0 C < T \le 1200^0 C \end{cases} \qquad (4)$$

Note that we have assumed that the normal part of the thermal strain and thermal stress in the transverse direction of the element is equal to zero (ε_{yth}=0 and σ_{yth}=0, see Fig. 2). A similar assumption also applies to mechanical stress and strain; in particular, the normal part of mechanical stress and mechanical strain are also ignored ($\varepsilon_y = 0, \sigma_y = 0$). This assumption is sometimes referred to as 'no interactive compression between longitudinal layers of the element' or 'the depth of the cross-section is constant after loading', which is a well-known and widely accepted hypothesis for beam analysis. Due to this assumption, only the longitudinal strain (ε_x) and the shear strain (γ) are considered as non-zero strain components of the beam element (see Fig. 3).

The total stress and strain condition at a point in reinforced concrete beam element can be represented by the Mohr circle (see Fig. 4).

The angle giving the orientation of the principal directions can then be defined according to

$$\tan 2\theta = -\frac{2\gamma}{\varepsilon_x} \rightarrow \theta \qquad (5)$$

The maximum value of principal strain is

$$\varepsilon_1 = \sqrt{\left(\frac{\varepsilon_x}{2}\right)^2 + (\gamma)^2} + \frac{\varepsilon_x}{2} \qquad (6)$$

The minimum value of principal strain is

$$\varepsilon_2 = -\sqrt{\left(\frac{\varepsilon_x}{2}\right)^2 + \left(\gamma\right)^2} + \frac{\varepsilon_x}{2} \tag{7}$$
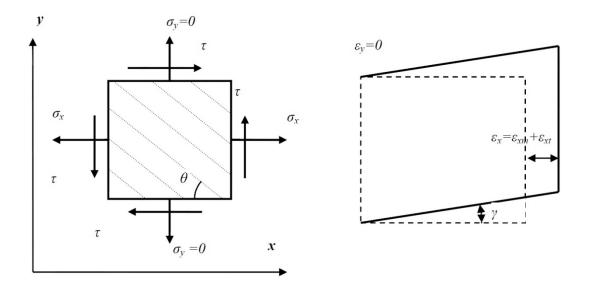
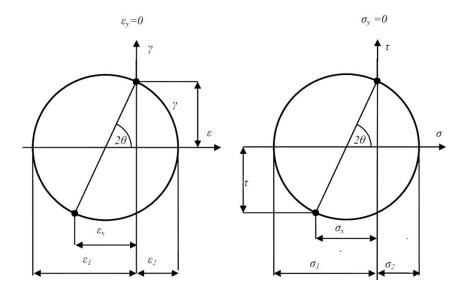Fig. 3 Total stress and strain condition at a position in beam element ($\varepsilon_y=0$ and $\sigma_y=0$)

Fig. 4 Mohr circle representation for strain and stress condition at a point in beam element

We note that in this case, the maximum strain is always positive and the minimum strain is always negative.

Once the strain components are known, we can compute the corresponding stress components by using the constitutive equation between principal stress and principal strain, assuming that the principal directions for strain and stress are the same. The latter is always the case for isotropic elastic response, and also for proper incremental damage parameterization (see Ibrahimbegovic and Frey (1993)). The constitutive equation between principal stress and principal strain of concrete and rebar is dependent on the temperature; it can be approximated by a number of mathematical equations (e.g., see Bentz *et al*. (2006), EN-1992-1-2 (2004), ACI-318 (2008), ASTM-E119 (2000), Le (2011), Vecchio and Collins (1988), or Nielsen, Pearce and Bicanic (2004)). In the following, some typical relationships are introduced:

Concrete

The mechanical stress-strain constitutive equation for concrete in compression can be computed by the following equation ASCE-1992 (1992) (see Fig. 5)

$$\sigma_{c2} = \begin{cases} f_c^{'}(T)\left[1-\left(\dfrac{\varepsilon_{c2}-\varepsilon_{max}(T)}{\varepsilon_{max}(T)}\right)^2\right] & for \quad \varepsilon_{c2} \leq \varepsilon_{max}(T) \\[4ex] f_c^{'}(T)\left[1-\left(\dfrac{\varepsilon_{max}(T)-\varepsilon_{c2}}{3\varepsilon_{max}(T)}\right)^2\right] & for \quad \varepsilon_{c2} > \varepsilon_{mex}(T) \end{cases} \qquad (8)$$

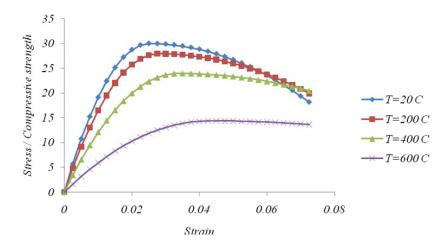where $\varepsilon_{max}(T) = 0.025 + \left(6T + 0.04T^2\right)\times 10^{-6}$

Fig. 5 Relation between compressive stress (MP) and strain of concrete due to tempeture ASCE-1992 (1992)

The compressive strength of concrete is dependent on temperature EN-1992-1-2 (2004)

$$f_c'(T) = \begin{cases} f_c' & for & T \leq 100^0 C \\ f_c'[1.067 - 0.00067T] & for & 100^0 C < T \leq 400^0 C \\ f_c'[1.44 - 0.0016T] & for & 400^0 C < T \leq 900^0 C \\ 0 & for & 900^0 C < T \end{cases} \tag{9}$$

where f_c' is the compressive strength of concrete at room temperature (20^0C)

The negative principal stress of concrete can also be computed from the negative principal strain by the equations of Vecchio and Collins (1988), which are widely used in American building codes ACI-318 (2008), AASHTO-LRFD (2012). In which, the minimum principal stress is computed by the equation

$$\sigma_{c2} = \sigma_{c2_{max}} \left(2 \frac{\varepsilon_{c2}}{\varepsilon_c'} - \left(\frac{\varepsilon_{c2}}{\varepsilon_c'} \right)^2 \right) \tag{10}$$

where

$$\sigma_{c2_{max}} = \left(\frac{1}{0.8 - 0.34 \dfrac{\varepsilon_{c1}}{\varepsilon_c'}} \right) f_c' \leq f_c' \tag{11}$$

The principal stress-strain relation of concrete in tension can be computed by following the suggestion of Vecchio and Collins (1988)

$$\sigma_{c1} = \begin{cases} E_c(T)\varepsilon_{c1} & if & \varepsilon_{c1} \leq \dfrac{f_{cr}(T)}{E_c(T)} \\ \dfrac{f_{cr}(T)}{1 + \sqrt{200\varepsilon_{c1}}} & if & \varepsilon_{c1} > \dfrac{f_{cr}(T)}{E_c(T)} \end{cases} \tag{12}$$

The Young modulus of concrete ($E_c(T)$) also depends on the temperature Nielsen *et al*. (2004)

$$E_c'(T) = E_c \left(1 - \left(\frac{T - 20}{10000} \right) \right)^2 \tag{13}$$

where E_c is the Young modulus of concrete at room temperature.

The crack limit of concrete in tension $f_{cr}(T)$ also depends on the temperature EN-1992-1-2 (2004)

$$f_{cr}(T) = \begin{cases} f_{cr} & if & T \leq 50^0C \\ f_{cr}(1 - 0.001356(T - 20)) & if & 50 < T \leq 640^0C \\ 0.2f_{cr} & if & 640 < T \leq 800^0C \\ 0 & if & T > 800^0C \end{cases} \tag{14}$$

where f_{cr} is the tension limit of concrete at room temperature and, if there is no experiment value, can be computed from the compressive strength of concrete ACI-318 (2008):

$$f_{cr} = 0.62\sqrt{f_c'}$$

Steel rebar

For reinforcement bar, a bi-linear mathematical model is usually used for both compression and tension condition (see Fig. 6)

$$f_s(T) = \begin{cases} E_s(T)\varepsilon_s & for & \varepsilon_s \leq 0.02 \\ f_y(T) & for & 0.02 < \varepsilon_s \end{cases} \tag{15}$$

The yield stress $f_y(T)$ of rebar is a function of the temperature (EN-1992-1-2 2004)

$$f_y(T) = \begin{cases} f_y & if & 0^0C \leq T \leq 350^0C \\ f_y\left[1.8848 - 2.528 \times 10^{-3}T\right] & if & 350^0C < T \leq 706^0C \\ f_y\left[0.242992764 - 2.02494 \times 10^{-4}T\right] & if & 706^0C < T \leq 1200^0C \end{cases} \tag{16}$$
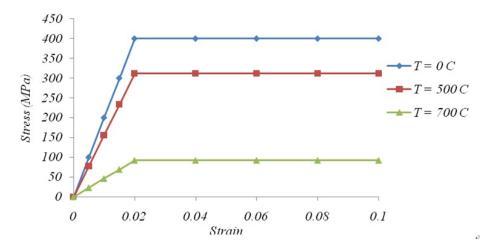

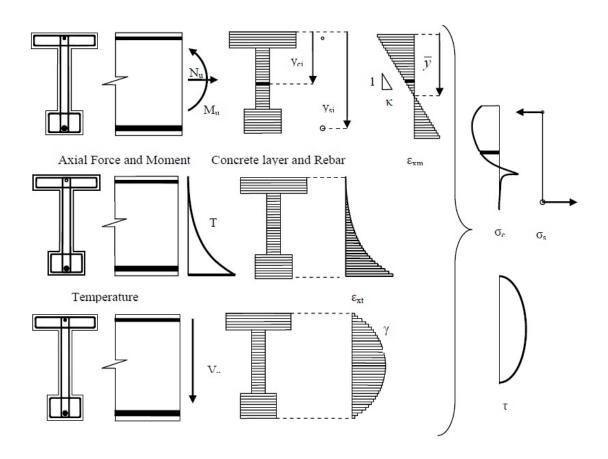Fig. 6 Stress- strain relationship of rebar in different temperature

By using the constitutive equation for concrete and steel rebar described above, we can obtain the principal stresses due to the principal strain, at a given considered position. Assuming isotropic elastic response implying that the principal stresses and the principal strains coincide, we can estimate the longitudinal normal stress (σ_x) and the shear stress (τ) by using the Mohr circle for stress condition (see Fig. 4)

The shear stress

$$\tau = \sqrt{(\sigma_1 - \sigma_2)^2} \sin(2\theta) \tag{17}$$

The longitudinal stress

$$\sigma_x = -\tau \tan(2\theta) \tag{18}$$

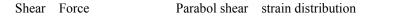Shear   Force   Parabol shear   strain distribution

Fig. 7 Response of reinforced concrete element under mechanical and thermal loads

Response of a reinforced concrete element under external loading and fire loading.

The mechanical response at the cross-section level is defined with respect to the generalized deformations (in the given section) represented by the curvature κ, the longitudinal strain ε_x at the middle of the section and the sectional shear deformation γ. We can further apply the 'layer' method Vecchio and Collins (1988), Hsu and Lin (2006), Kodur and Dwaikat (2008), where the cross-section is divided into a number of layers across the beam depth. Each layer is assumed to be thin enough to allow for uniform distributions of stress, strain and temperature (see Fig. 7).

We denote the layer width and height as b_{ci} and h_{ci}, the longitudinal stress as σ_{cxi} and the distance from the middle of the layer to the top of the cross-section of concrete layer 'i^{th}' as y_{ci}; furthermore, we denote the steel bar area a_{sxj}, the longitudinal stress σ_{sxj} and the distance from the middle of the rebar element to the top of the cross section of the rebar element 'j^{th}' as y_{sj}, we can establish the following set of equilibrium equations

$$\begin{cases} \sum_{i=1}^{N_c} \sigma_{cxi} b_{ci} h_{ci} + \sum_{j=1}^{Ns} \sigma_{sxj} a_{sxj} = N \\ \sum_{i=1}^{N_c} \sigma_{cxi} b_{ci} h_{ci} (y_{ci} - \bar{y}) + \sum_{j=1}^{N_s} \sigma_{sxj} a_{sxj} (y_{sj} - \bar{y}) = M \\ \sum_{i=1}^{N_c} \tau_i b_i h_i = V \end{cases} \qquad (19)$$

where $\bar{y}$ is the distance from the neutral axis (where $\varepsilon_x = 0$) to the top of the cross-section.

This system allows us to compute the response of the cross-section, and in particular curvature, longitudinal strain and shear deformation, at a given force and temperature loads; the following procedure is used (see Fig. 8):

2.3 Effect of temperature loading, axial force and shear load on mechanical moment-curvature response of reinforced concrete beam element

By applying the procedure illustrated in Fig. 8, we can establish the moment-curvature relation for a reinforced concrete beam element, by fixing the temperature loading, the shear loading, the axial force and tracking the increase of the internal moment (*M*) proportional to the increase of the curvature (κ).

Fig. 11 shows the degradation of the moment-curvature response of a rectangular reinforced concrete beam exposed to ASTM 119 fire acting on the bottom (see Fig. 9) in case external axial force and shear force equal to zero (pure bending test) ($N_u = 0$, $V_u = 0$). The temperature profile of the RC beam subjected to fire loading increases due to time (see Fig. 10), set according to ASTM-E119 (2000). With increase of temperature, the strength of materials, both concrete and rebar, will decrease and lead to the degradation of moment-curvature resistance of the element.
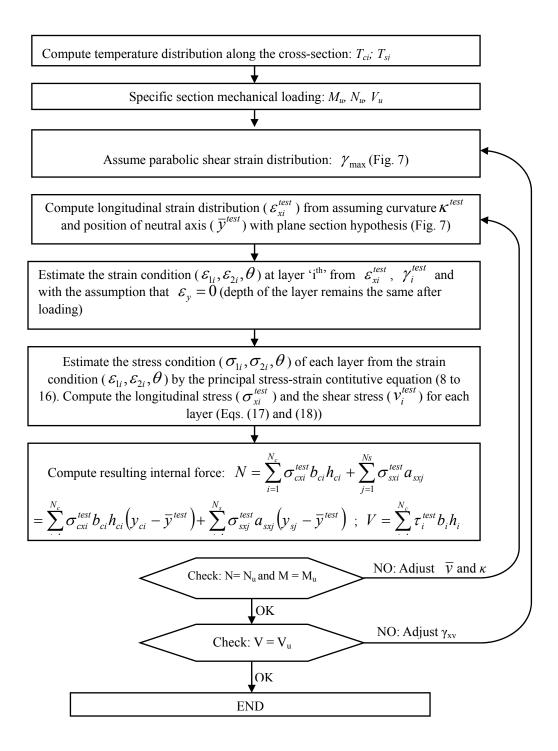
Fig. 8 Procedure to determine the mechanical response of RC beam element
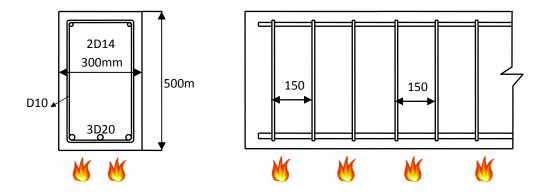
Fig. 9 Cross-section and Dimensioning of the considered reinforced concrete element
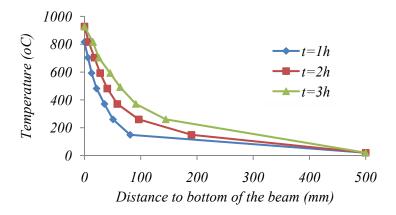
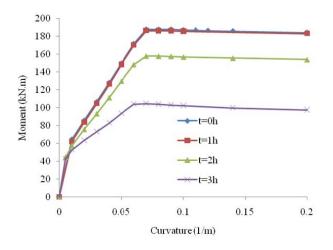Fig. 10 Evolution of temperature profile with time ASTM-E119 (2000)

Fig. 11 Dependence of moment-curvature curve with time exposure to ASTM 119 fire
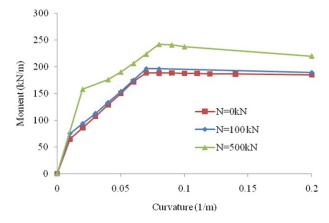
Fig. 12 Dependence of moment-curvature on axial compression
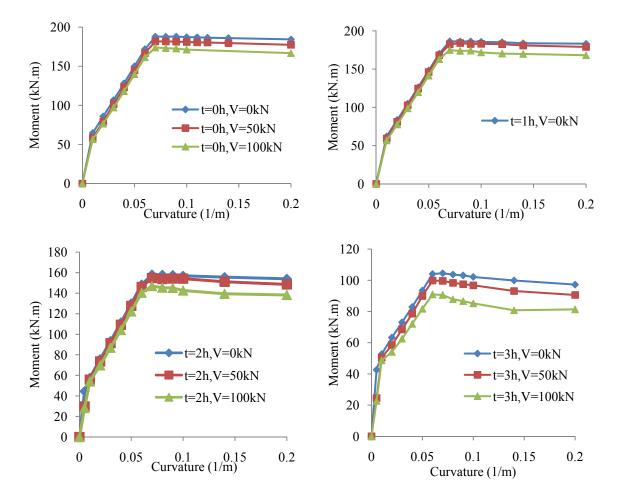

Fig. 13 Dependence of moment-curvature response on shear loading

Fig. 12 illustrates the evolution of bending resistance of the frame with an increase of the axial compression.

Fig. 13 expresses the reduction of the bending resistance when shear load increases at four instants: t =0h, t=1h, t=2h and t=3h.

In Figs. 11 to 13, we have indicated that the moment-curvature diagram can approximately be represented in a multi-linear form (see Ibrahimbegovic and Frey (1993)) with the 'crack' moment M_c, the 'yield moment' M_y, the 'ultimate' moment M_u and the corresponding values of curvature: κ_c, κ_y, κ_u. The 'crack' moment is obtained at the state where the tensile fiber of concrete starts to crack. The 'yield' moment is the moment acting on the cross section to make the tensile rebar starts to yield. The peak resistance of the beam is reached when both the tensile rebar yields and the concrete the compressive fiber collapses to make the 'ultimate' bearing state of the beam. From this state on, the 'bending hinge' occurs at the cross-section and the bending resistance of the cross-section starts to decrease with further curvature increase (see Fig. 14).
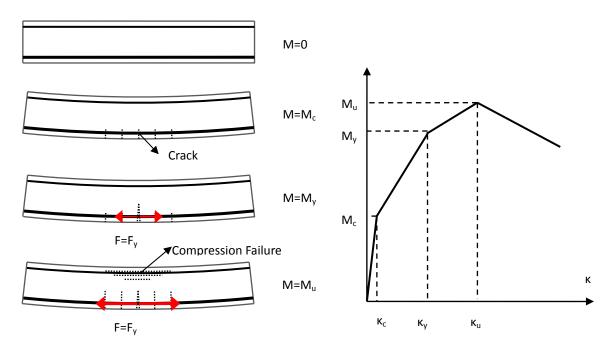

Fig. 14 Multi-linear moment-curvature model of the reinforced concrete beam in bending

2.4 Mechanical shear load – shear strain response of a reinforced concrete element subjected to pure shear loading under elevated temperature

There can be several positions in frame structures where moment and axial force are small enough in comparison to shear force (for example, at the place on the top of the pin support), at such a position, the failure of the frame is due to shear force rather than bending moment. The shear strength of reinforced concrete element is normally assumed to be the total of the concrete

component and stirrups component; it can be computed by the proposed general algorithm shown in Fig. 8 or by applying the compression field theory. In this theory, the shear resistance of the beam is considered by assuming that the longitudinal strain of the cross-section is equal to zero. This model implies that the angle of the principal stress and strain is equal to 45^0C

$$\tan 2\theta = -\frac{2\gamma}{\varepsilon_x = 0} \rightarrow \tan 2\theta = \infty \rightarrow \theta = 45^0 \tag{20}$$

The maximum and the minimum strains are opposite in sign and equal in magnitude

$$\varepsilon_1 = \sqrt{\left(\frac{\varepsilon_x = 0}{2}\right)^2 + (\gamma)^2} + \frac{\varepsilon_x = 0}{2} \rightarrow \varepsilon_1 = \gamma \tag{21}$$

$$\varepsilon_2 = -\sqrt{\left(\frac{\varepsilon_x = 0}{2}\right)^2 + (\gamma)^2} + \frac{\varepsilon_x = 0}{2} \rightarrow \varepsilon_2 = -\gamma \tag{22}$$

The principal stress can be computed from the principal strain for concrete and steel bar by applying Eqs. (8) to (16). The shear stress can therefore be computed from the shear strain and the temperature at each concrete layer and/or rebar element

$$\tau_i = \sigma_{1i} = f(\varepsilon_{1i}, T_i) = f(\gamma_i, T_i) \tag{23}$$

The equilibrium equation for shear force

$$V_u = V_c + V_s = \sum_{i=1}^{N_c} \tau_{ci} b_{ci} h_{ci} + \frac{d \cot an(\theta)}{s} A_{sv} \sigma_{sv} \tag{24}$$

Where d is the 'effective' depth of reinforced concrete cross section subjected to shear load, s is the stirrups' spacing, A_{sv} is the area of stirrup and σ_{sv} is the stress in the stirrups corresponding to the considered shear strain. For pure shear test ($\theta = 45^0$), the result (24) becomes

$$V_u = V_c + V_s = \sum_{i=1}^{N_c} \tau_{ci} b_{ci} h_{ci} + \frac{d}{s} A_{sv} \sigma_{sv} \tag{25}$$

From the (23) to (25), we can estimate the corresponding shear force (V_u) of a given shear deformation (γ), which allows us to draw the shear force – shear strain diagram in a given cross-section.

Fig. 15 shows the reduction of shear resistance of the RC element given in Fig. 15 when subjected to ASTM 119 fire.

With a similar approximation already used for the moment-curvature curve, we also introduce a multi-linear response for the shear resistance of a reinforced concrete element (see Fig. 15 for illustration). In the next section, we show how to apply these stress-resultant models in the finite element analysis of reinforced concrete frame structure subjected to combined mechanical and thermal loads, by using the Timoshenko beam element.
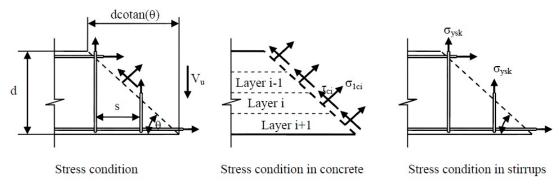
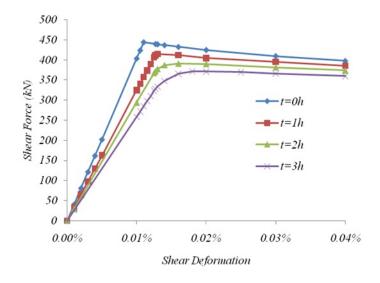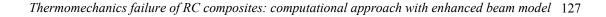Fig. 15 Stress components of reinforced concrete subjected to pure shear loading

Fig. 16 Mechanical shear force- shear deformation diagram

3. Finite element analysis of reinforced concrete frame

The moment-curvature curve and the shear force-shear strain diagram of reinforced concrete beam exposed to fire loading can be represented by the Timoshenko beam model. It can consider both the hardening response while micro-cracks develop in fracture process zone and the softening behavior of the element once the micro-cracks coalesence happen in producing a macro crack. This model was first developed for bending-dominated failure modes in Pham *et al.* (2010, 2013). These developments are summarized in the following section, and then further extended to account for shear-dominated failure modes.

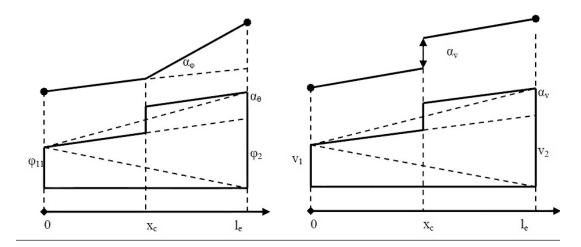### 3.1 Kinematic equation of Timoshenko beam with strong discontinuities

Fig. 17 Discontinuity in rotation and vertical displacement

In this model, localized failure due to either bending and/or shear is assumed to happen at the local point x_c. The corresponding failure modes are represented by 'jumps' in either rotation, for bending failure, or vertical displacement, for shear failure (see Fig. 16). In the presence of failure mode, the displacement field is decomposed into a regular part and a discontinuous part as

$$\mathbf{u}(x) = \overline{\mathbf{u}}(x) + \boldsymbol{\alpha} \mathrm{H}_{x_c} = \begin{bmatrix} \overline{u}(x) \\ \overline{v}(x) \\ \overline{\varphi}(x) \end{bmatrix} + \begin{bmatrix} 0 \\ \alpha_v \\ \alpha_\varphi \end{bmatrix} \mathrm{H}_{x_c} \tag{26}$$

where H_{x_c} denotes the Heaviside function, which is equal to zero when $x < x_c$ and is equal to one when $x \geq x_c$; whereas $\boldsymbol{\alpha} = \begin{pmatrix} 0 & \alpha_v & \alpha_\theta \end{pmatrix}^T$ denotes the vector of discontinuities in the local point x_c.

If we introduce a regular differentiable function $\phi(x)$ being 0 at x = 0 and 1 at x = l, the displacement field can then be rewritten as

$$\mathbf{u}(x) = \underbrace{\left[\overline{\mathbf{u}}(x) + \boldsymbol{\alpha}\phi(x) \right]}_{\widetilde{\mathbf{u}}(x)} + \boldsymbol{\alpha} \underbrace{\left[\mathrm{H}_{x_c}(x) - \phi(x) \right]}_{M(x)} \tag{27}$$

The corresponding deformation field is then computed

$$\boldsymbol{\varepsilon}(x) = \boldsymbol{\varepsilon}(\widetilde{\mathbf{u}})(x) + \boldsymbol{\alpha}\mathbf{G}(x) + \boldsymbol{\alpha}\delta_{x_c}(x) \tag{28}$$

where $\mathbf{G}$ is equal to $\mathbf{L}(-\phi)(x)$ (with $\mathbf{L}$ being the strain-displacement operator) and $\delta_{x_c}(x)$ is the Dirac delta function.

3.2 Stress-resultant constitutive model for reinforced concrete element

3.2.1 Bending model

The bending behavior of a reinforced concrete beam is represented by the relation between the internal moment (M) and the corresponding curvature (κ). In this article, a multi-threshold isotropic plasticity model Pham *et al.* (2010, 2013) is chosen to represent that kind of behavior.

The curvature is consider to be the composition of 'elastic' part and 'plastic' part

$$\kappa = \kappa^e + \kappa^p \tag{29}$$

In continuum regime, the bending behavior of the beam is controlled by a Helmholtz free energy

$$\psi\left(\kappa^e, \xi\right) = \frac{1}{2}\kappa^e EI \kappa^e + \Xi(\xi) \tag{27}$$

where ξ is the internal variable controlling the plastic hardening of the material.

The plastic threshold is chosen as

$$\Phi(M, q) = |M| - \left(M_y - q\right) \tag{28}$$

where q is the 'stress-like' variable controlling the evolution of the threshold.

The constitutive equations are obtained by applying the second principle of thermodynamics for the elastic case

$$M = EI\left(\kappa - \kappa^p\right) = EI\kappa^e \;\; ; \;\; q = -KI\xi \tag{29}$$

Moreover, considering that these constitutive equations remain valid in the inelastic case, we can further obtain the evolution equations for internal variables by appealnig to the maximum dissipation principle

$$\dot{\kappa}^p = \dot{\lambda}\frac{\partial\Phi}{\partial M} = \dot{\lambda}sign(M) \qquad ; \;\; \dot{\xi} = \dot{\lambda}\frac{\partial\Phi}{\partial q} = \dot{\lambda} \tag{30}$$

The rate form of consitutive equation between internal moment and the curvature will finaly be computed

$$\dot{M} = \begin{cases} EI\dot{\kappa} & \dot{\lambda} = 0 \\ \dfrac{EIKI}{EI + KI}\dot{\kappa} & \dot{\lambda} > 0 \end{cases} \tag{31}$$

along with the loading/unloading conditions $\dot{\lambda}\Phi = 0, \dot{\lambda} \geq 0, \Phi \leq 0$ and consistency condition $\dot{\lambda}\Phi = 0$.

For the proposed model for reinforce concrete beam, two plasticity thresholds should be taken into account. The first threshold: $\Phi_c\left(M, q_c\right) = |M| - \left(M_c - q_c\right)$ where M_c is the elastic limit which corresponds to the state in which the concrete in the tension part starts to crack with isotropic hardening $q_c = -K_1 I\xi$. The second threshold: $\Phi_y\left(M, q_y\right) = |M| - \left(M_y - q_y\right)$ where

M_y is the plastic limit which corresponds to the state in which the steel bar starts to yield with isotropic hardening $q_y = -K_2 I \xi$

To describe the softening part of internal moment at the 'plastic' hinge, a rigid-plastic model is introduced:

$$\overline{\overline{\Phi}}\left(M_{x_c}, \overline{\overline{q}}\right) = \left|M_{x_c}\right| - \left(M_u - \overline{\overline{q}}\right) \le 0 \tag{32}$$

where M_{x_c} is the moment at the failure point, M_u is ultimated moment of reinforced concrete section.

The isotropic behavior is chosen for the softening threshold: $\overline{\overline{q}} = -\overline{\overline{K}} I \overline{\overline{\xi}}$ with $\overline{\overline{K}} < 0$

Note that due to the rigid behavior of the plastic hinge at x_c, the equivalent total strain α_φ and the plastic strain are equal, and α_φ can thus be interpreted as a plastic strain; its evolution is given by:

$$\dot{\alpha}_\theta = \dot{\overline{\overline{\lambda}}} \frac{\partial \overline{\overline{\Phi}}}{\partial M} = \dot{\overline{\overline{\lambda}}} \, sign(M) \qquad and \qquad \dot{\overline{\overline{\xi}}} = \dot{\overline{\overline{\lambda}}} \frac{\partial \overline{\overline{\Phi}}}{\partial \overline{\overline{q}}} = \dot{\overline{\overline{\lambda}}} \tag{33}$$

The bulk and discontinuity behavior is described in Fig. 17, which is similar to what had been explained in Fig. 14. All the parameters of the model can be identified by the layer method as already explained in Section 2.
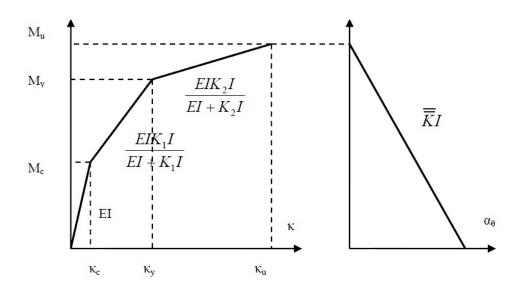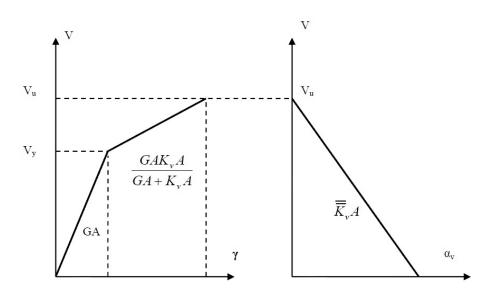

Fig. 18 Moment-curvature relation for bending stress-strain model

3.2.2 Shear model

Fig. 19 Shear load - shear strain relation for shear stress-resultant model

The shear strength of a reinforced concrete beam consists of two mains ingredients: the contribution of concrete (V_c) and the contribution of stirrups (V_s). The shear behavior of a beam therefore undergoes over three stages. The first stage have the highest strength since the shear response come from both concrete and stirrups. Once the concrete is failure, the shear behavior moves to the second stage where the shear strength comes from stirrups only. The last stage kicks off in case both the stirrups and the concrete are failure. In this stage, the shear behavior is no longer increase and starts to reduce.

In this article, the shear behavior is also modeled by a multi-linear elasto-plastic model (see Fig. 18). Main equations are summaried in the following:

The decomposition of the shear strain

$$\gamma = \gamma^e + \gamma^p \tag{34}$$

The continuum shear behavior is controlled by the free energy

$$\psi_v\left(\gamma^e, \xi_v\right) = \frac{1}{2}\gamma^e GA \gamma^e + \Xi_v\left(\xi_v\right) \tag{35}$$

The yield threshold for the cross section

$$\Phi_v\left(V, q_v\right) = V - \left(V_y - q_v\right) \leq 0 \tag{36}$$

The state equations

$$V = GA\left(\gamma - \gamma^p\right) = GA\gamma^e \tag{37}$$

$$q_v = -K_v A \xi_v \tag{38}$$

where q_v is the 'stress-like' variable controlling the hardening at plastic regime.

The evolution equations

$$\dot{\gamma}^p = \dot{\lambda}_v \frac{\partial \Phi_v}{\partial V} = \dot{\lambda}_v sign(V) \qquad and \qquad \dot{\xi}_v = \dot{\lambda}_v \frac{\partial \Phi_v}{\partial q_v} = \dot{\lambda}_v \tag{39}$$

The constitutive equation in continuum shear behavior

$$\dot{V} = \begin{cases} GA\dot{\gamma} & \dot{\lambda}_v = 0 \\ \dfrac{GAK_vA}{GA+K_vA}\dot{\gamma} & \dot{\lambda}_v > 0 \end{cases} \tag{40}$$

The softening part of the behavior is described by and a threshold function at the failure point

$$\overline{\overline{\Phi}}\left(V_{x_c}, \overline{\overline{q}}_v\right) = \left|V_{x_c}\right| - \left(V_u - \overline{\overline{q}}_v\right) \le 0 \tag{41}$$

with isotropic softening

$$\overline{\overline{q}}_v = \overline{\overline{K}}_v A \overline{\overline{\xi}}_v \qquad with \qquad \overline{\overline{K}}_v < 0 \tag{42}$$

3.3 Equilibrium equation

We consider a beam summitted to external loads and fire as described in Fig.
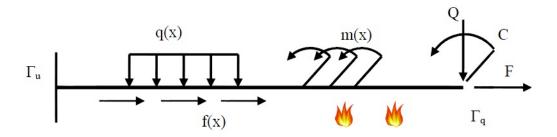

Fig. 20 Beam under external loading and fire

Denoting as N, V and M respectively the internal axial force, transverse shear force and bending moment, the strong form of the local equilibrium can be written as

$$\begin{cases} \dfrac{dN}{dx} + f(x) = 0 \\[2mm] \dfrac{dV}{dx} + q(x) = 0 \\[2mm] \dfrac{dM}{dx} + T(x) + m(x) = 0 \end{cases} \qquad \rightarrow \dfrac{d\boldsymbol{\sigma}}{dx} + \mathbf{f}(x) = 0 \qquad (43)$$

The corresponding weak form for the standard Timoshenko beam model becomes

$$\int_0^l \boldsymbol{\sigma}^T \varepsilon(\mathbf{w})\,dx = \int_0^l f^T \mathbf{B}\,dx + F^T \mathbf{w} \qquad (44)$$

where $\boldsymbol{\sigma}$ is the stress-resultant vector ($\boldsymbol{\sigma} = \begin{bmatrix} N & V & M \end{bmatrix}^T$), $\mathbf{w}$ is a virtual generalized displacement ($\mathbf{w} \in V_0$ where $V_0 = \left\{ \mathbf{w} : [0,l] \rightarrow R^3 \,\middle|\, \mathbf{w} \in H^1([0,l]) \, and \, \mathbf{w} = 0 \, on \, \Gamma_u \right\}$), $\mathbf{f} = (f,q,m)^T$ is the vector of distributed load $\mathbf{F} = (F,Q,C)^T$ the vector of concentrated forces.

3.4 Finite element approximation

Note that from (27), the displacement field is the composition of the regular part and the singular part: $\mathbf{u}(x) = \widetilde{\mathbf{u}}(x) + \boldsymbol{\alpha}\left[\mathrm{H}_{x_c}(x) - \phi(x) \right]$

We choose the isoparametric interpolation functions for the regular part of displacement field $\widetilde{\mathbf{u}}(x)$

$$\widetilde{\mathbf{u}}^h(x) = \begin{bmatrix} \widetilde{u}^h(x) = N_1(x)u_1 + N_2(x)u_2 \\ \widetilde{v}^h(x) = N_1(x)v_1 + N_2(x)v_2 \\ \widetilde{\varphi}^h(x) = N_1(x)\varphi_1 + N_2(x)\varphi_2 \end{bmatrix} = \mathbf{N}(x)\mathbf{d} \qquad (45)$$

where

$$\mathbf{N}(x) = \begin{bmatrix} N_1(x) & & & N_2(x) & & \\ & N_1(x) & & & N_2(x) & \\ & & N_1(x) & & & N_2(x) \end{bmatrix} \; with \; N_1(x) = 1 - \frac{x}{l^e}; N_2(x) = \frac{x}{l^e} \quad (46)$$

and $\mathbf{d}$ is the vector of nodal displacements: $\mathbf{d} = \begin{bmatrix} u_1 & v_1 & \varphi_1 & u_2 & v_2 & \varphi_2 \end{bmatrix}^T$

Furthermore, by choosing $N_2(x)$ for the function $\phi(x)$ (see Fig. 20), the general displacement field can finally be re-written

$$\mathbf{u}^h(x) = \mathbf{N}\mathbf{d} + \boldsymbol{\alpha}\left(\mathrm{H}_{x_c}(x) - N_2(x) \right) \qquad (47)$$

The strain field of the beam is computed from the displacement field by using the Timoshenko kinematic equation

$$\boldsymbol{\varepsilon}(x) = \left(\begin{array}{c} \varepsilon(x) = \dfrac{\partial u}{\partial x} \\[2mm] \gamma(x) = \dfrac{\partial v}{\partial x} - \varphi(x) \\[2mm] \kappa(x) = \dfrac{\partial \varphi}{\partial x} \end{array}\right) \tag{48}$$

$$\rightarrow \boldsymbol{\varepsilon}^h(x) = \mathbf{B}(x)\mathbf{d} + \mathbf{G}_r(x)\boldsymbol{\alpha} = \mathbf{B}(x)\mathbf{d} + \overline{\mathbf{G}}_r(x)\boldsymbol{\alpha} + \boldsymbol{\alpha}\delta_{x_c} \tag{49}$$

where

$$\mathbf{B} = \begin{bmatrix} B_1 & 0 & 0 & B_2 & 0 & 0 \\ 0 & B_1 & -N_1 & 0 & B_2 & -N_2 \\ 0 & 0 & B_1 & 0 & 0 & B_2 \end{bmatrix}; \quad \overline{\mathbf{G}}_r(x) = \begin{bmatrix} -B_2 & 0 & 0 \\ 0 & -B_2 & 0 \\ 0 & 0 & -B_2 \end{bmatrix} \tag{50}$$

and δ_{x_c} is the Dirac delta function.

To build the weak form of the equibrilium equation, we use the same interpolation functions for the virtual strain field $\boldsymbol{\varepsilon}^*(x)$

$$\boldsymbol{\varepsilon}^*(x) = \mathbf{B}(x)\mathbf{d}^* + \mathbf{G}_v(x)\boldsymbol{\beta}^* = \mathbf{B}(x)\mathbf{d}^* + \overline{\mathbf{G}}_v(x)\boldsymbol{\beta}^* + \boldsymbol{\beta}^*\delta_{x_c} \tag{51}$$

where $\mathbf{d}^*$ and $\boldsymbol{\beta}^*$ are the virtual nodal displacement and virtual displacement jump, respectively.
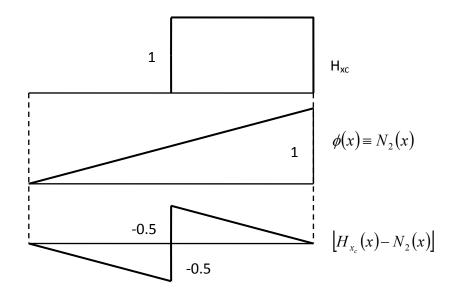

Fig. 21 Heaviside function H_{x_c} and $\phi(x)$

Function $\mathbf{G}_v$ is chosen in the framework of the incompatible mode method of Ibrahimbegovic and Wilson (1991)

$$\mathbf{G}_v(x) = \mathbf{G}_r(x) - \frac{1}{l^e} \int_0^{l^e} \mathbf{G}_r(x) dx \qquad (52)$$

For Timoshenko beam element with only one integration point: $\mathbf{G}_v(x) = \mathbf{G}_r(x)$. With such interpolations, the weak form of equilibrium Eq. (45) leads to a system

$$\forall \mathbf{d}^*, \forall \boldsymbol{\beta}^* \begin{cases} \int_0^l \mathbf{d}^* \mathbf{B}^T \boldsymbol{\sigma} dx = \int_0^l \mathbf{d}^* \mathbf{N}^T \mathbf{f} dx + \mathbf{d}^* \mathbf{F} \\ \int_0^{l^e} \boldsymbol{\beta}^* \overline{\mathbf{G}}_v^T \boldsymbol{\sigma} dx + \boldsymbol{\sigma}\big|_{x_c} = 0 \qquad \forall e \in \left[1, N_{elem}^\alpha\right] \end{cases} \qquad (53)$$

The system (53) can be re-written in the form where the standard set of global equilibrium equations for finite element method is accompanied by the element-based equations

$$\begin{cases} \overset{N_{elem}}{\underset{e=1}{A}} \left[\mathbf{f}^{e,\text{int}} - \mathbf{f}^{e,ext}\right] = 0 \\ \mathbf{h}^e = \int_0^{l^e} \overline{\mathbf{G}}_v^T \boldsymbol{\sigma} dx + \boldsymbol{\sigma}\big|_{x_c} = 0 \qquad \forall e \in \left[1, N_{elm}^\alpha\right] \end{cases} \qquad (54)$$

where

$$\mathbf{f}^{e,\text{int}} = \int_0^{l^e} \mathbf{B}^T \boldsymbol{\sigma} dx \;, \qquad \mathbf{f}^{e,ext} = \int_0^{l^e} \mathbf{N}^T \mathbf{f} dx + \mathbf{F} \qquad (55)$$

also, $\mathbf{N}_{elem}^\alpha$ denotes the set of elements enriched with a discontinuity and $\boldsymbol{\sigma}\big|_{x_c}$ represents the value of the stress-resultant vector at point x_c where the discontinuity is introduced: $\boldsymbol{\sigma}\big|_{x_c} = \int_0^{l^e} \boldsymbol{\sigma} \delta_{x_c}$

Denoting as i the iteration for time step $n+1$ of Newton's iterative procedure and providing the corresponding iterative updates $\Delta \mathbf{d}_{n+1}^{(i)} = \mathbf{d}_{n+1}^{(i+1)} - \mathbf{d}_{n+1}^{(i)}$ and $\Delta \boldsymbol{\alpha}_{n+1}^{(i)} = \boldsymbol{\alpha}_{n+1}^{(i+1)} - \boldsymbol{\alpha}_{n+1}^{(i)}$, the system (53) can be re-written in the linearized form

$$\begin{cases} \overset{N_{elem}}{\underset{e=1}{A}} \left[\mathbf{K}_{n+1}^{e,(i)} \Delta \mathbf{d}_{n+1}^{(i)} + \mathbf{F}_{r,n+1}^{e,(i)} \Delta \boldsymbol{\alpha}_{n+1}^{(i)}\right] = \overset{N_{elem}}{\underset{e=1}{A}} \left[\mathbf{f}_{n+1}^{e,ext} - \mathbf{f}_{n+1}^{e,\text{int}(i)}\right] \\ \mathbf{h}_{n+1}^{e,(i)} + \left(\mathbf{F}_{v,n+1}^{e,(i)} + \mathbf{K}_{\mathbf{d},n+1}^{(i)}\right) \Delta \mathbf{d}_{n+1}^{(i)} + \left(\mathbf{H}_{n+1}^{e,(i)} + \mathbf{K}_{\alpha,n+1}^{(i)}\right) \Delta \boldsymbol{\alpha}_{n+1}^{(i)} = 0 \end{cases} \qquad (56)$$

where the following notations is used

$$\mathbf{K}_{n+1}^{e,(i)} = \int\limits_0^{l^e} \mathbf{B}^T \mathbf{C}_{n+1}^{an,(i)} \mathbf{B} dx \qquad\qquad \mathbf{F}_{r,n+1}^{e,(i)} = \int\limits_0^{l^e} \mathbf{B}^T \mathbf{C}_{n+1}^{an,(i)} \overline{\mathbf{G}}_r dx$$

$$\mathbf{F}_{v,n+1}^{e,(i)} = \int\limits_0^{l^e} \overline{\mathbf{G}}_v^T \mathbf{C}_{n+1}^{an,(i)} \mathbf{B} dx \qquad\qquad \mathbf{H}_{n+1}^{e,(i)} = \int\limits_0^{l^e} \overline{\mathbf{G}}_v^T \mathbf{C}_{n+1}^{an,(i)} \overline{\mathbf{G}}_r dx$$

We also denote with $\mathbf{K}_{\mathbf{d},n+1}^{(i)}$ and $\mathbf{K}_{\boldsymbol{\alpha},n+1}^{(i)}$ the consistent tangent stiffness for the discontinuity part

$$\Delta\boldsymbol{\sigma}\Big|_{x_c,n+1}^{(i)} = \mathbf{K}_{d,n+1}^{(i)} \Delta\mathbf{d}_{n+1}^{(i)} + \mathbf{K}_{\alpha,n+1}^{(i)} \Delta\boldsymbol{\alpha}_{n+1}^{(i)} \tag{57}$$

and $\mathbf{C}_{n+1}^{an,(i)}$ denotes the consistent tangent modulus for the bulk material obtained as a discretized version of the tangent modulus given in Eqs. (31) and (40)

$$\Delta\boldsymbol{\sigma}_{n+1}^{(i)} = \mathbf{C}_{n+1}^{an,(i)} \Delta\boldsymbol{\varepsilon}_{n+1}^{(i)} \tag{58}$$

where $\boldsymbol{\sigma}$ and $\boldsymbol{\varepsilon}$ the generalized stress and strain, respectively.

The system (56) is solved by an operator split procedure (see Brancherie and Ibrahimbegovic (2009) and Ibrahimbegovic (2009)). In which, the second equation (concerning the local equilibrium for the element with active failure mode) is solved first at the element level for a given nodal displacement increment $\Delta\mathbf{d}_{n+1}^{(i)}$ to determine the increment of displacement 'jump' $\Delta\boldsymbol{\alpha}_{n+1}^{(i)}$. Once the increment of displacement 'jump' $\Delta\boldsymbol{\alpha}_{n+1}^{(i)}$ is known, we then perform the static condensation of at the element level, and carry on to solve the increment of displacement from the first equation. The static condesation of the system (56) can be written

$$\overset{N_{elem}}{\underset{e=1}{A}} \left[\hat{\mathbf{K}}_{n+1}^{e,(i)} \Delta\mathbf{d}_{n+1}^{(i)} \right] = \overset{N_{elem}}{\underset{e=1}{A}} \left[\mathbf{f}_{n+1}^{e,ext} - \mathbf{f}_{n+1}^{e,\text{int}(i)} \right] \tag{59}$$

where

$$\hat{\mathbf{K}}_{n+1}^{e,(i)} = \left\{ \mathbf{K}_{n+1}^{e,(i)} + \mathbf{F}_{r,n+1}^{e,(i)} \left(\mathbf{H}_{n+1}^{e,(i)} + \mathbf{K}_{\alpha,n+1}^{(i)} \right)^{-1} \left(\mathbf{F}_{v,n+1}^{e,(i)} + \mathbf{K}_{d,n+1}^{(i)} \right) \right\} \tag{60}$$

is the 'modified' element tangent modulus.

4. Numerical examples

4.1 Four-point bending test

We consider here a simple reinforced concrete beam subjected to ASTM 119 fire (see ASTM-E119 (2000)) at its bottom and external mechanical load applied in the vertical direction as described in Fig. 21.

The beam is composed by carbonate concrete with compressive strength $f_c' = 30 MPa$. Two longitudinal reinforcement bars of diameter 14 mm are placed at the top the cross section and three longitudinal reinforcement bars of diameter 20 mm are placed at the bottom. The concrete cover

thickness is 40 mm. The beam is also transversely reinforced by stirrups of diameter 10 mm with the spacing of 125 mm. The yield limit of steel is 400MPa.

Using the layer method described in section 2, we can identify the stress-resultant models for bending failure and shear failure at different instants of fire loading program (Figs. 22 and 23).
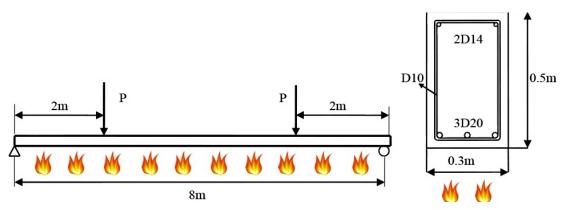

Fig. 22 Simple reinforced concrete beam subjected to ASTM 119 fire and vertical forces
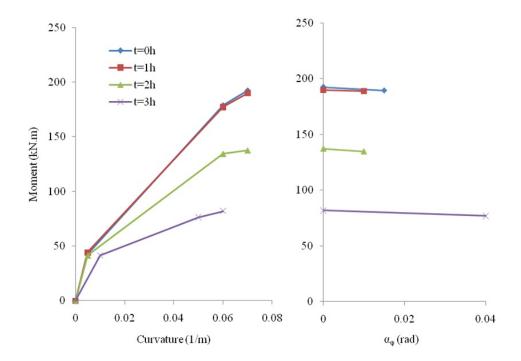

Fig. 23 Reduction of bending resistance due to time exposure to fire ASTM 119

The corresponding values of material parameters for bending model are given in Table 2.

Table 2 Bending model parameters for different instants of fire loading program

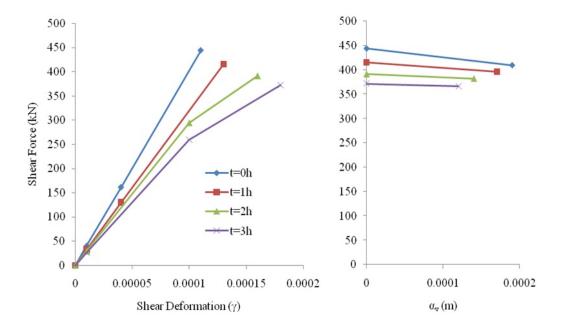| Parameters	t =0h	t =1h	t =2h	t=3h
Young Modulus E (kN/m^2)	2708121	2835722	2644230	1324882
Hardening Modulus K_1 (kN/m^2)	795440.3	773984.9	540969.6	279660.4
Hardening Modulus K_2(kN/m^2)	433372.2	404203.2	99201.84	177893.4
Softening Modulus $\overline{\overline{K}}$ (kN/m)	-66943.8	-34230.2	-79727.8	-40232.5
Crack shear M_c (kNm)	42.3144	44.30815	41.3161	41.40257
Yield shear M_y (kNm)	87.15347	177.3368	134.2953	76.36012
Ultimate shear M_u (kNm)	192.5736	189.9682	137.3953	81.91929

Fig. 24 Reduction of shear resistance due to time exposure to fire ASTM 119

The corresponding parameters for shear failure model are presented in Table 3.

Table 3 Parameters of shear model at different instants of fire loading program

Parameters	t =0h	t =1h	t =2h	t=3h
Shear Modulus G (kN/m²)	26892218	21686667	19600983	17267528
Hardening Modulus K_1 (kN/m²)	26892218	21690899	19520350	17267528
Hardening Modulus K_2(kN/m²)	26892218	21114573	3850031	8273086
Softening Modulus $\bar{\bar{K}}$ (kN/m²)	-1208592	-743844	-444255	-310832
Crack shear V_c (kN)	40.33833	32.53	29.40148	25.90129
Yield shear V_y (kN)	161.3533	130.139	371.9836	284.9142
Ultimate shear V_u (kN)	443.7216	415.1858	391.0413	371.7816

Fig. 24 shows the relation between the load P and the deflection in the middle of the beam exposed to fire loading at times t=0h, t=1h, t=2h and t=3h.
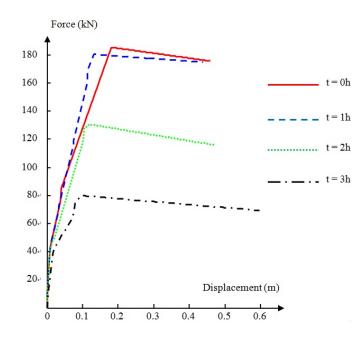

Fig. 25 Force/displacement curve of the beam at different instants of fire loading program

We note that after a long exposure to fire loading, the bearing resistance of the beam is significantly reduced. In particular, after one hour fire exposure, the ultimate load of the beam reduces from 185.27 kN to 180.31 kN; then after two hours, the ultimate load reduces to 130.48 kN and it finally reduces to 79.767 kN after three hours of exposure to ASTM 119 fire (see Fig. 25).
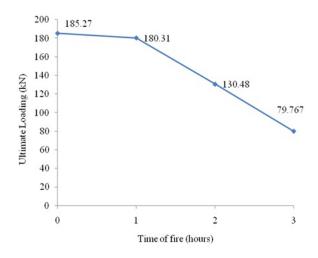

Fig. 26 Reduction of ultimate load due to fire exposure

4.2 Reinforced concrete frame subjected to fire

We consider a two-storey frame with the geometry given in Fig. 26. The material properties are listed in the Table 4. Each of the two columns of the frame is subjected to a compressive load equal to 700 kN acting on the top of the column. A horizontal force Q acts on the left edge of the second storey leading to a horizontal displacement of the frame. Two reinforced concrete beams corresponding to the spans of the frame are submitted to ASTM119 standard fire (ASTM-E119 2000) on their bottom. Fig. 27 shows the evolution of temperature of the beam that has been submitted to fire for one, two and three hours.

Table 4 Material Properties

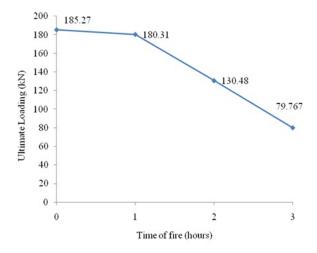| Concrete Properties			
Modulus of Elasticity	E_c	26889.6	N/mm^2
Compression Strength	f_{cc}	30	N/mm^2
Steel Properties			
Yield Stress	f_{sy}	400	N/mm^2
Modulus of Elasticity	E_s	20000	N/mm^2

Fig. 27 Two-story reinforced concrete frame subjected to loading and fire
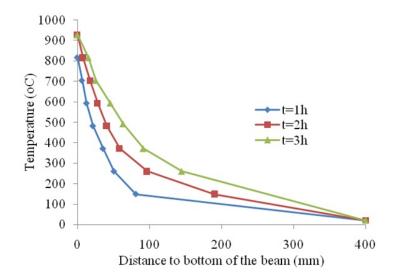

Fig. 28 Temperature profile of the reinforced concrete beam due to time of fire

Since the columns are highly compressed with a 700kN force, their bending resistance is much greater than the bending resistance of the beam. The bending model of the column at room temperature (no fire acting) is given in Fig. 28.
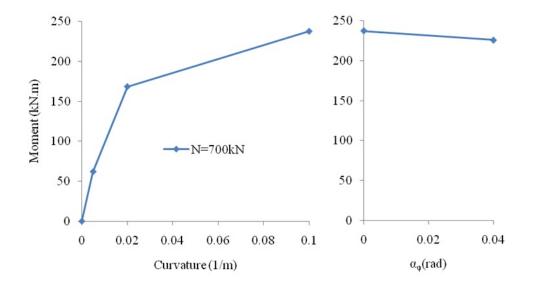
Fig. 29 Moment-curvature model for the column
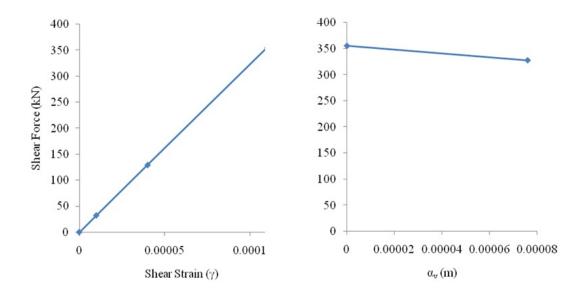
The shear model of the column is given in Fig. 29

Fig. 30 Shear failure model for the column

Fig. 30 represents the degradation of moment-curvature curve of the beam after one, two and three hours exposing to fire.
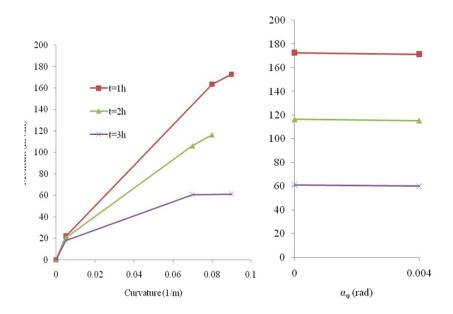

Fig. 31 Degradation of bending resistance of reinforced concrete beam versus fire exposure
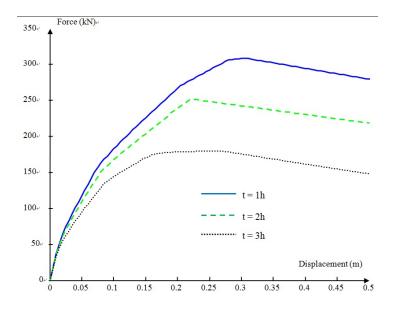

Fig. 32 Horizontal force/displacement curve of two-story frame at different instants of fire

Fig. 31 illustrates the reduction of the overall response of the frame due to fire by plotting the relationship between horizontal force Q with the horizontal displacement of the top beam at different times: t= 1 hour, t = 2 hours and t = 3 hours.

We can note, in particular, that the ultimate horizontal load of the reinforced concrete frame decreases from 308.52kN to 251.46kN and then to 180.01kN after one hour, two hours and three hours submitted to fire. This is the result of the degradation of the material properties due to high temperature and also due to the thermal effect on the beam.

5. Conclusions

In this work we have developed a method to calculate the behavior of reinforced concrete frame structure subjected to fire, with combined thermal and mechanical loads. The main novelty of the proposed method is that is its capability of taking into account the thermal loading and the degradation of material properties due to the temperature in determining the ultimate load of the reinforced concrete frame. Moreover, in the proposed method we consider not only the bending failure but also the shear failure of the reinforced concrete structure. This is also a new contribution in solving the resistance of reinforced concrete frame exposure to fire and thermal effect.

The finite element approach presented for this kind of problem can deal with the localized failure of the reinforced concrete structure. Two most frequent failure mechanisms are treated separately in order to provide the most robust computational procedure. The numerical examples we have presented here confirmed a very satisfying results provided by proposed methodology.

This proposed strategy is a first step towards fully coupled thermomechanical problems to achieve reliable description of the structural resistance all along the exposure to the thermal loading.

Extending the proposed formulation to geometrically nonlinear framework can be accomplished by following the footsteps indicated in Ibrahimbegovic *et al*. (2013) and Ngo *et al*. (2014). Another possible line of development will concern combining the proposed structural model with refined material modeling of concrete under fire, such as elaborated upon by (Ostermann and Dinkler 2014, Cramer *et al*. 2014).

Acknowledgments

References

AASHTO-LRFD (2012), *AASHTO LRFD Bridge Design Specifications.* Highway Subcommittee on Bridges and Structures.
ACI-216 (1997), *Standard method for determining fire resistance of concrete and mansonry construction assemblies*, American Concrete Institute.

ACI-318 (2008), *Building code requirements for structural concrete and commentary*, American Concrete Institute.

ASCE (1992), *Structural fire protection*, New York: ASCE Manual and Reports on Engineering Practice.

ASTM-E119 (2000), *Standard test methods for fire tests of building construction and material*, American Society for Testing and Materials.

Bentz, D., Vecchio, F.J. and Collins, M.P. (2006), "Simplifed modified compression field theory for calculating shear strength of reinforced concrete elements", *ACI Struct. J.*, **103**(65), 614-624.

Brancherie, D. and Ibrahimbegovic, A. (2009), "Novel anisotropic continuum-discrete damage model capable of representing localized failure of massive structures. Part I: theoretical formulation and numerical", *Int. J. Comput. Aided Eng. Softw.*, **26**, 100-127.

Capua, D.D. and Mari, A.R. (2007), "Nonlinear analysis of reinforced concrete cross-section exposed to fire", *Fire Safety J.*, **103**(4), 139-149.

Cramer, F., Kowalsky, U. and Dinkler, D. (2014), "Coupled chemical and mechanical processes in concrete structures with respect to aging", *Coupled Syst. Mech.*, **3**(1), 53-71.

Dwaikat, M. and Kodur, V.K.P. (2008), "A numerical approach for modeling the fire induced restraint effects in reinforced concrete beams", *Fire Safety J.*, **43**, 291-307.

EN-1992-1-2 (2000), *Eurocode 2: design of concrete structure - Part 1-2: general rules- structural fire design*, Eurocode.

Hsu, J.H. and Lin, C.S. (2006), "Residual bearing capabilities of fire-exposed reinforced concrete beams", *Int. J. Appl. Sci. Eng.*, **4**, 151-163.

Ibrahimbegovic, A. (2009), *Nonlinear solid mechanics: theoretical formulation and finite element solution methods*, Springer.

Ibrahimbegovic, A. and Wilson, E.L. (1991), "A modified method of incompatible modes", *Commun. Appl. Mech.Method.*, 187-194.

Ibrahimbegovic, A. and Frey, F. (1993), "Stress resultant finite element analysis of reinforced concrete plates", *Eng. Comput.*, **10**(1), 15-30.

Ibrahimbegovic, A., Hajdo, E. and Dolarevic, S. (2013), "Linear instability or buckling problems for mechanical and coupled thermomechanical extreme conditions", *Coupled Syst. Mech.*, **2**(4), 349-374.

Kodur, V.K.P. and Dwaikat, M. (2008), "A numerical model for predicting the fire resistance of reinforced concrete beams", *Cement Concrete Compos.*, **30**(5), 431-443.

Le, T.T.H. (2011), *Etude multi-échelles du comportement Thermo-Hydro-Mécanique des matériaux cimentaires*, *Approche morphologique pour la prise en compte de la mésostructure.* France: Université Paris-Est.

Nielsen, C.V., Chris, J.P. and Nenad, B. (2004), "Improved phonomenological modelling of transient thermal strains for concrete at high temperatures", *Comput. Concrete.*, **1**, 189-209.

Ngo, V.M., Ibrahimbegovic, A. and Hajdo, E. (2014), "Nonlinear instability problems including localized plastic failure and large deformations for extreme thermomechanical load", *Coupled Syst. Mech.*, **3**(1), 89-110.

Ostermann, L. and Dinkler, D. (2014), "Modelling and numerical simulation of concrete structures subject to high temperatures", *Coupled Syst. Mech.*, **3**(1), 72-110.

Pham, B.H., Davenne, L., Brancherie, D. and Ibrahimbegovic, A. (2010), "Stress resultant model for ultimate load design of reinforced concrete frames: combined axial force and bending moment", *Comput. Concrete*, 303-315.

Pham, B.H., Brancherie, D., Davenne, L. and Ibrahimbegovic, A. (2013), "Stress-resultant models for ultimate load design of reinforced concrete frames and multi-scale parameter estimates", *Comput. Mech.*, **51**(3), 347-360.

Vecchio, F.J. and Collins, M.P. (1992), "Predicting the response of reinforced concrete beams subjected to shear using compression field theory", *ACI Struct. J.*, **1988**, 258-268.

Vecchio, F.J. and Emara, M.B. (1993), "Shear deformation in reinforced concrete frames", *ACI Struct. J.*, 46-56.

Vecchio, F.J. and Collins, M.P. (1988), "Predicting the response of reinforced concrete beams subjected to shear using compression field theory", *ACI Structural Journal.*, 258-268.

Xavier, H.F.B. (2009), *Analysis of reinforced concrete frames exposed to fire: based on advanced calculation methods*, Porto: Universidade do Porto.